CHAPTER V

RESULTS AND DISCUSSION

The results and discussion in this chapter are divided into three sections. Section 5.1 is described characteristics and catalytic properties of crystattlite sizes of titanium (IV) oxide (titania) obtained in this work were synthesized from Titanium tert-butoxide (TNB) mixed with organic solvents, toluene, in an autoclave under autogenous pressure (Sornnarong Theinkaew, 2000: 70). Section 5.2 is explained effect of crystallite sizes of titania on 20 wt% Co/TiO_2 catalysts. Finally, effect of crystallite size of titania on various Co loading catalysts for CO hydrogenation is illustrated in section 5.3.

5.1 Formation of Titanium (IV) oxide

5.1.1 Crystallite size of titania

Titanium (IV) oxide has been synthesized in toluene at various conditions (Solvothermal Method). Under inert organic solvent condition, thermal decomposition of TNB in toluene was occurred, yielding a $\equiv Ti\text{-}O^-$ anion. The nucleophilic attack of the titanate ion on another ion and crystallization was taken place, finally yielding the anatase titania. The mechanism of TNB in toluene can be depicted as shown in Figureure 5.1.

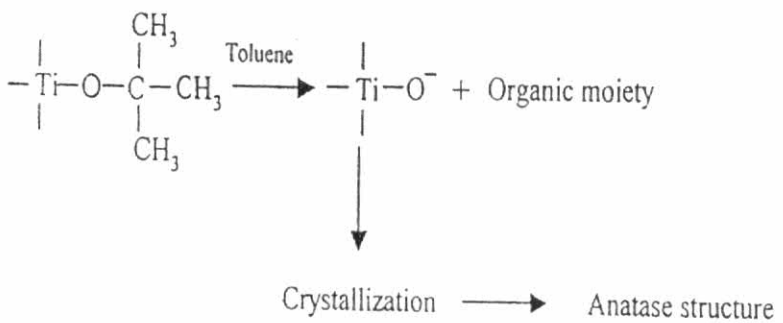

Figure 5.1 Mechanism of reaction in toluene for the titania product (Sornnarong Theinkeaw, 2000: 71).

5.1.2 X-ray diffraction (XRD) and Specific surface area

Titania was synthesized for various conditions as show in Table 5.1. From XRD pattern, the crystallite size of the anatase samples was calculated from the half-height width of the 101 diffraction peak of anatase using the Scherrer equation.

Table 5.1 Specific surface areas and average crystallite sizes of the TiO_2 samples obtained from various synthesis conditions

Sample	Amount of TNB in solvent (g)	Temperature (°C)	Holding time (h)	Crystallite Size (nm)	Specific surface area (m^2/g)		S_1/S_2
					S_1[a]	S_2[b]	
1	15	300	0.5	9.0	126.4	170.9	0.74
2	25	300	2.0	11.0	92.3	139.9	0.66
3	25	320	6.0	12.5	78.2	123.1	0.64
4	25	350	6.0	14.5	53.1	106.1	0.50
5	25	350	8.0	15.0	51.1	102.6	0.50

[a] S_1 is specific surface area determined from N_2 physisorption results.

[b] S_2 is specific surface area calculated based on the correlation between surface area and crystallite size of TiO_2 ($S_2 = \frac{6}{d\rho}$ [26]).

The crystallite size of the solvothermal-derived TiO_2 was varied in the range of 9-15 nm by changing the concentrations of TNB, the reaction temperatures, and the holding times. Increasing reaction temperature and holding time resulted in an increase in the average crystallite size of TiO_2. The average crystallite sizes and BET surface areas of the obtained TiO_2 from various synthesis conditions are given in **Table 5.1**. The XRD patterns of all the obtained TiO_2 powders are shown in **Figure 5.2**. The characteristic peaks of pure anatase phase titania were observed at 25, 38, and 48° 2θ [Watson *et al.* (2003)] without contamination of other phases such as rutile and brookite. The average crystallite sizes of TiO_2 were calculated from the full width at half maximum of the XRD peak at $2\theta = 25°$ using the Scherrer equation. As the average TiO_2 crystallite size increased from 9 to 15 nm, the BET surface areas

decreased monotonically from 126 to 51 m^2/g. The specific surface areas of the TiO_2 samples were also calculated based on the correlation between surface area and crystallite size as follows:

$$S_2 = \frac{6}{d\rho}$$

where d is the average crystallite size and ρ is the density of TiO_2 (3.84 g cm^{-3}) [Payakgul *et al.* (2005)].

It is noticed that S_1 determined from N_2 physisorption was smaller than S_2 calculated based on the crystallite size for all the TiO_2 samples. This was probably the results of an amorphous-like phase contaminated in the TiO_2 particles [Kominami *et al.* (1999)].

5.1.3 Electron microscopy

Transmission electron microscope imaging has been carried out in order to determine the shape of the particles and the existence of amorphous phase. A typical TEM micrograph of the TiO_2-9 nm sample is shown in **Figure 5.3**. The TEM images show that the TiO_2 products obtained by solvothermal method under there conditions consist of spherical particles with particle sizes consistent with the calculated from XRD results. The TiO_2 samples may contain a fraction of amorphous since the preferential orientation of TiO_2 nanoparticles was not clearly seen; however, it is probably due to the moderate magnification used. In order to elucidate the structure of TiO_2 nanocrystallites, a high-resolution transmission electron microscope with selected area electron diffraction (SAED) may be needed.

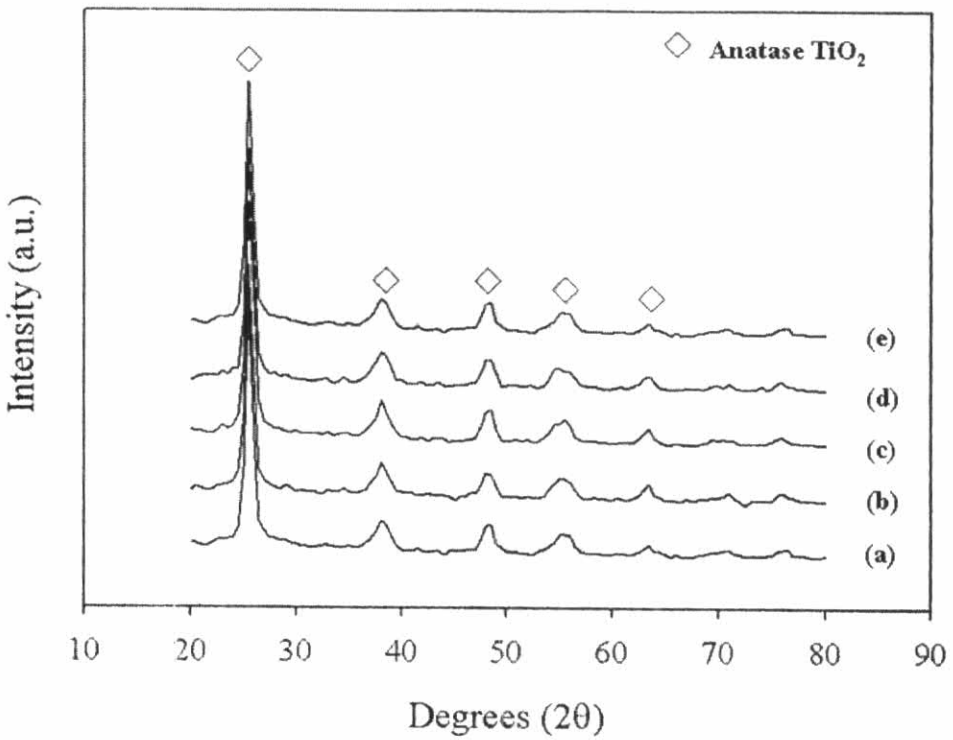

Figure 5.2 XRD patterns of the TiO_2 samples with various crystallite sizes (a) 9 nm (b) 11 nm (c) 12.5 nm (d) 14.5 nm and (e) 15 nm.

(a)

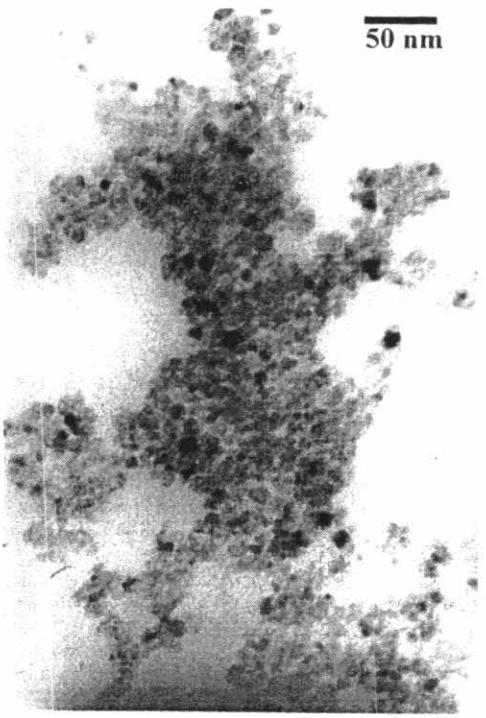

(b)

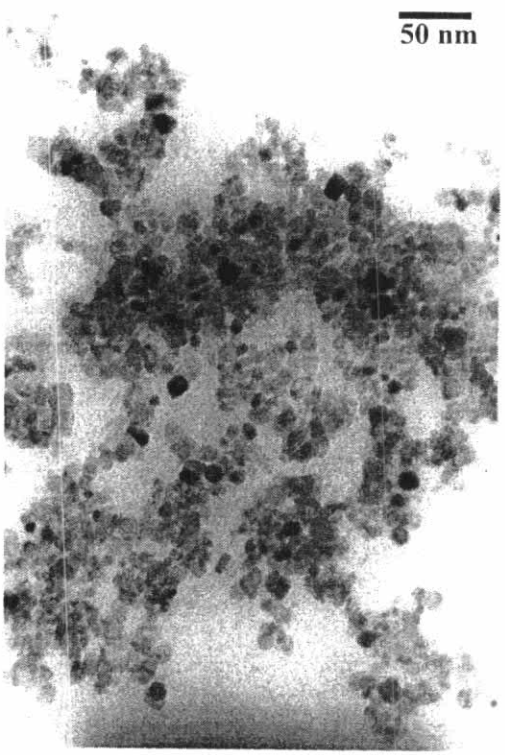

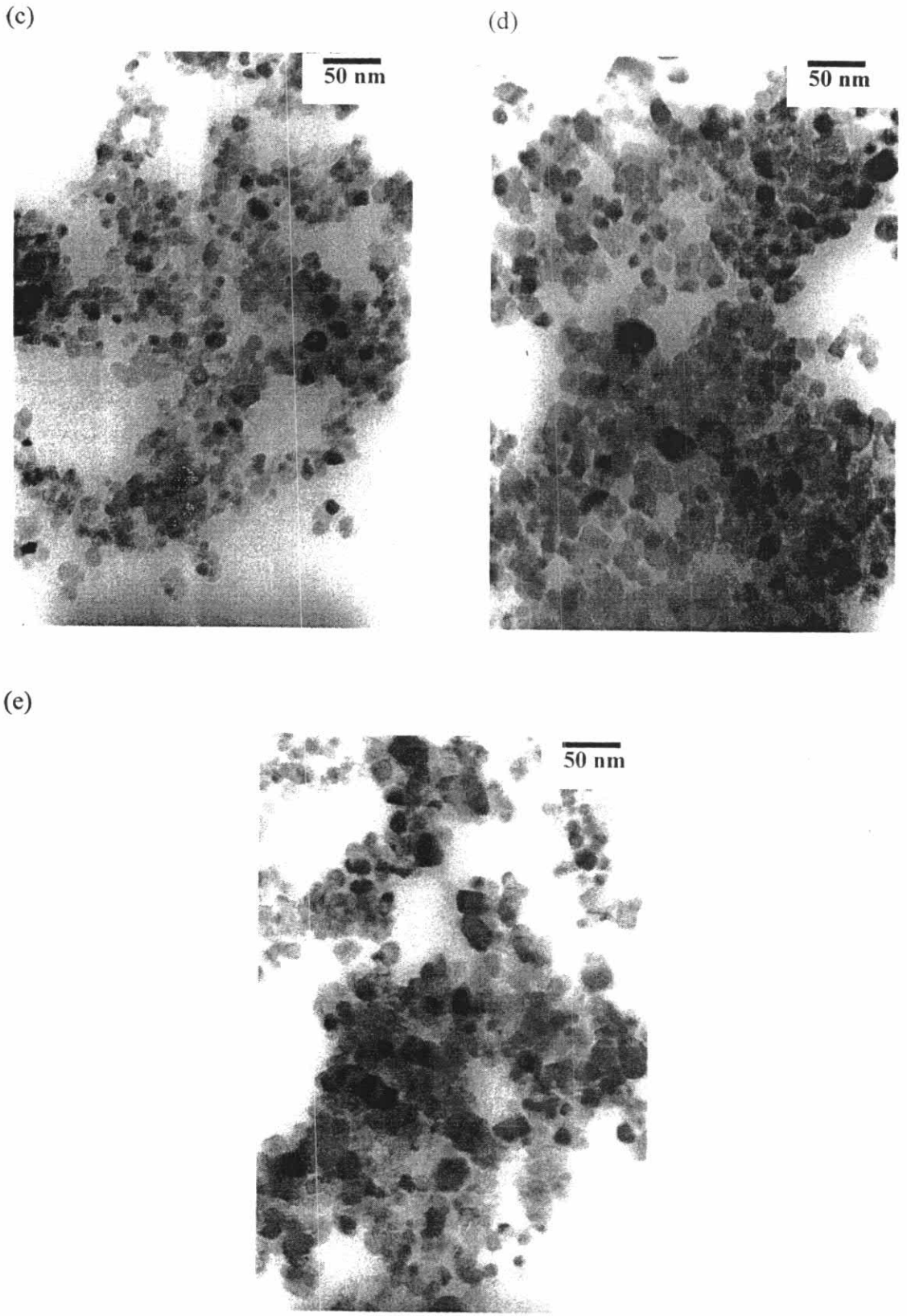

Figure 5.3 A typical TEM micrograph of the TiO_2-(a) 9 nm (b) 11 nm samples (c) 12.5 nm (d) 14.5 nm and (e) 15 nm samples.

5.1.4 Temperature programmed desorption

Temperature programmed desorption profiles of CO_2 from the titania surface are shown in **Figure 5.4**. The titania samples exhibited two desorption peaks at temperatures ca. 183 K and 213 K which were attributed to the two structures of TiO_2 [Tracy *et al.* (2003)]. The peak at ca. 183 K is attributed to CO_2 molecules bounding to regular five-coordinate Ti^{4+} site which was considered as the perfected titania structure. The second peak at ca. 213 K has been considered as desorption of CO_2 molecules bounding to Ti^{3+} defect structure. It is clearly seen from the TPD results that the areas of the CO_2 desorption peak at 213 K apparently increased with increasing crystallite size. It is indicated that the larger crystallite size of TiO_2 obtained from solvothermal synthesis possessed higher amount of Ti^{3+} surface defects. The ratios of peak areas of Ti^{3+}/Ti^{4+} were also determined by curve fitting and area calculation using a SYSTAT Peakfit program and the results are given in **Table 5.2**. It was found that the Ti^{3+} density increased with increasing TiO_2 crystallite size from 9 nm to 14.5 nm. The value of Ti^{3+}/Ti^{4+} for TiO_2-14.5 nm and TiO_2-15 nm was not significantly different.

Table 5.2 The ratios of peak areas of Ti^{3+}/Ti^{4+} determined from the CO_2-TPD experiments

Average crystallite size[a] (nm)	Ti^{3+}/Ti^{4+}[b]
9.0	0.923
11.0	1.046
12.5	1.299
14.5	1.580
15.0	1.474

[a] Based on XRD results
[b] Based on CO_2-TPD results.

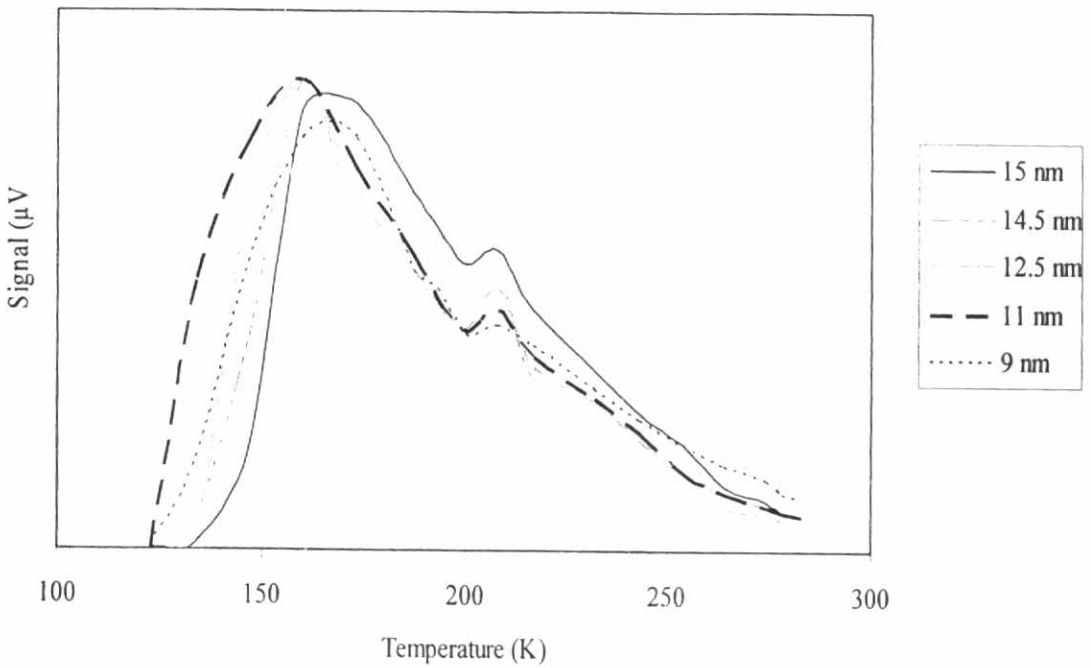

Figure 5.4 Thermal desorption spectra for CO_2 adsorbed on the various TiO_2 samples

5.1.5 Electron spin resonance

An example of the ESR results of the solvothermal-derived TiO_2 powders is shown in **Figure 5.5**. All the titania samples exhibited one major signal at *g* value of 1.996 which can be assigned to Ti^{3+} at titania surface [Park *et al.* (1999), Watterich *et al.* (1996), Zeng *et al.* (2002)]. According to Nakaoka et al. (1997), there were six ESR signals that occurred on the surface of titania: (i) $Ti^{4+}O^{-}Ti^{4+}OH^{-}$, (ii) surface Ti^{3+}, (iii) adsorbed oxygen (O^{2-}), (iv) $Ti^{4+}O^{2-}Ti^{4+}O^{2-}$, (v) inner Ti^{3+}, and (vi) adsorbed water. **Figure 5.6** demonstrates a relationship between the intensity of ESR spectra per surface area of the TiO_2 and the TiO_2 average crystallite size. It was found that the amount of surface defect of TiO_2 increased with increasing crystallite size.

(a)

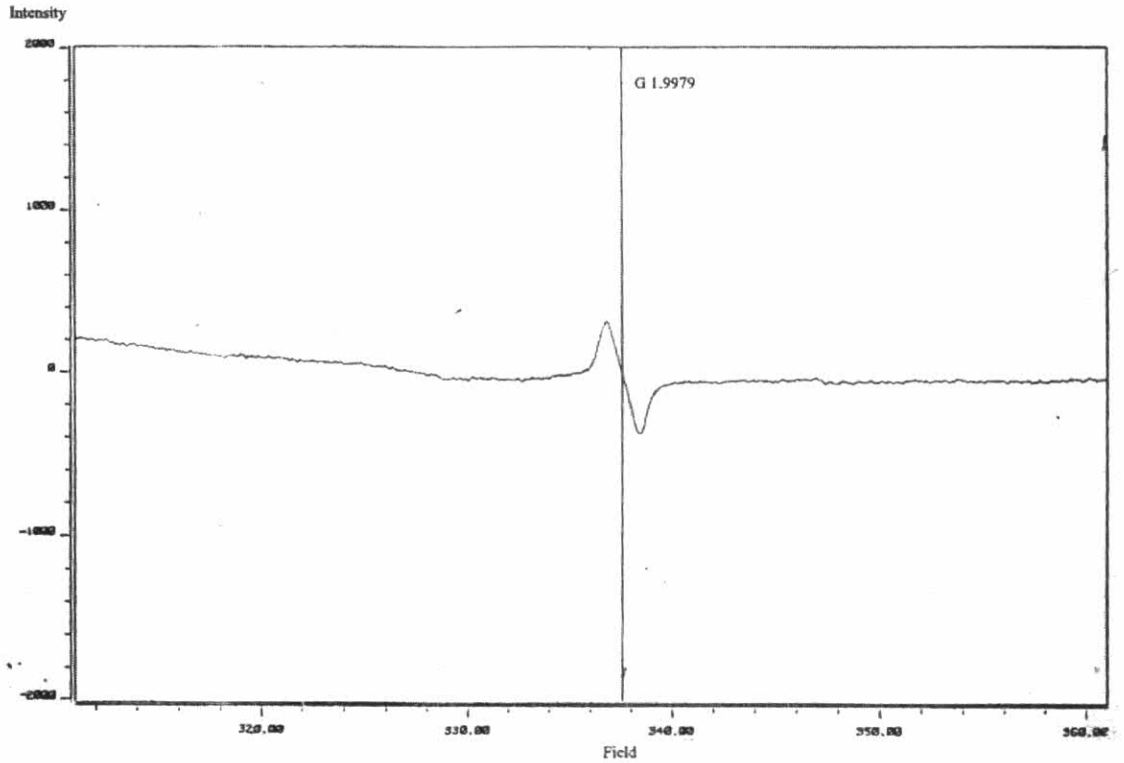

(b)

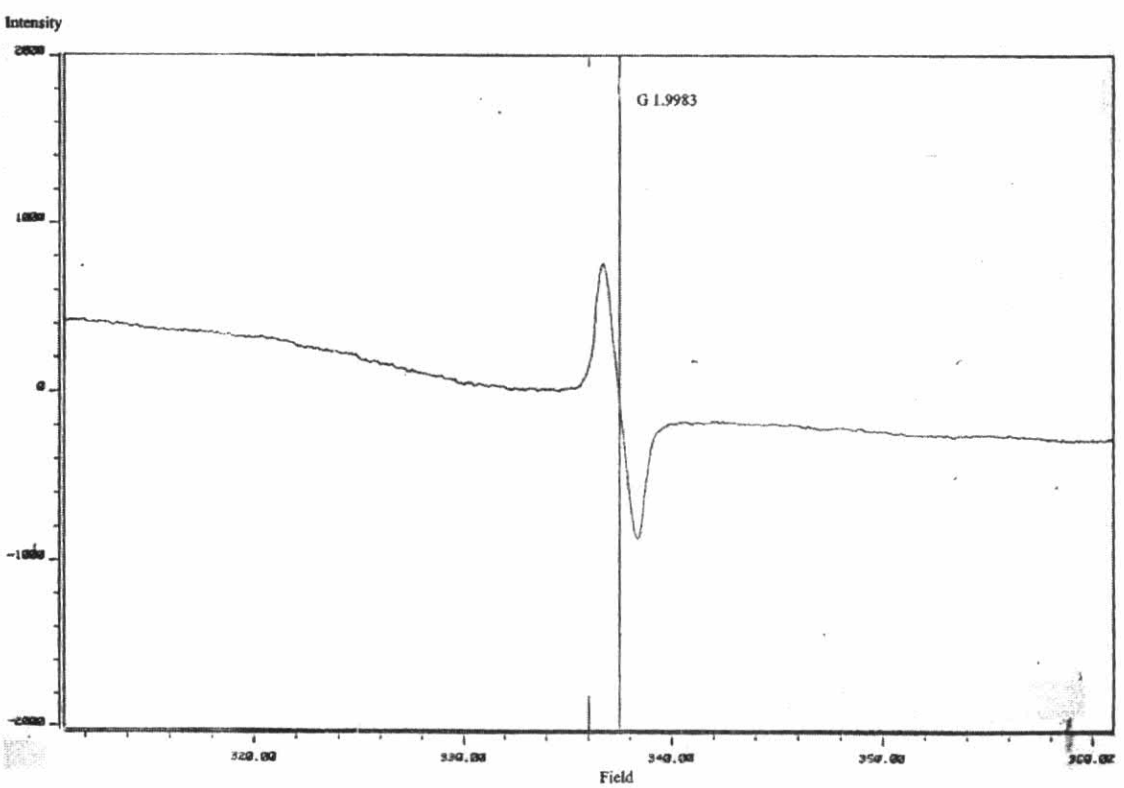

(c)

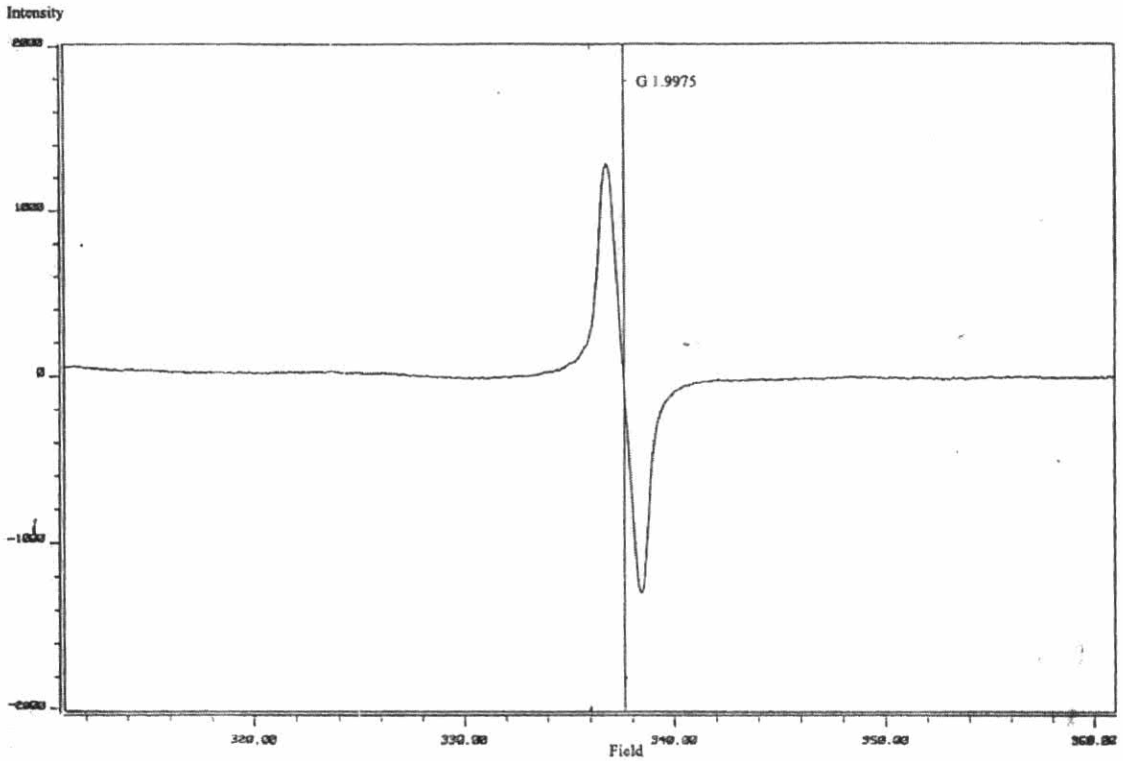

(d)

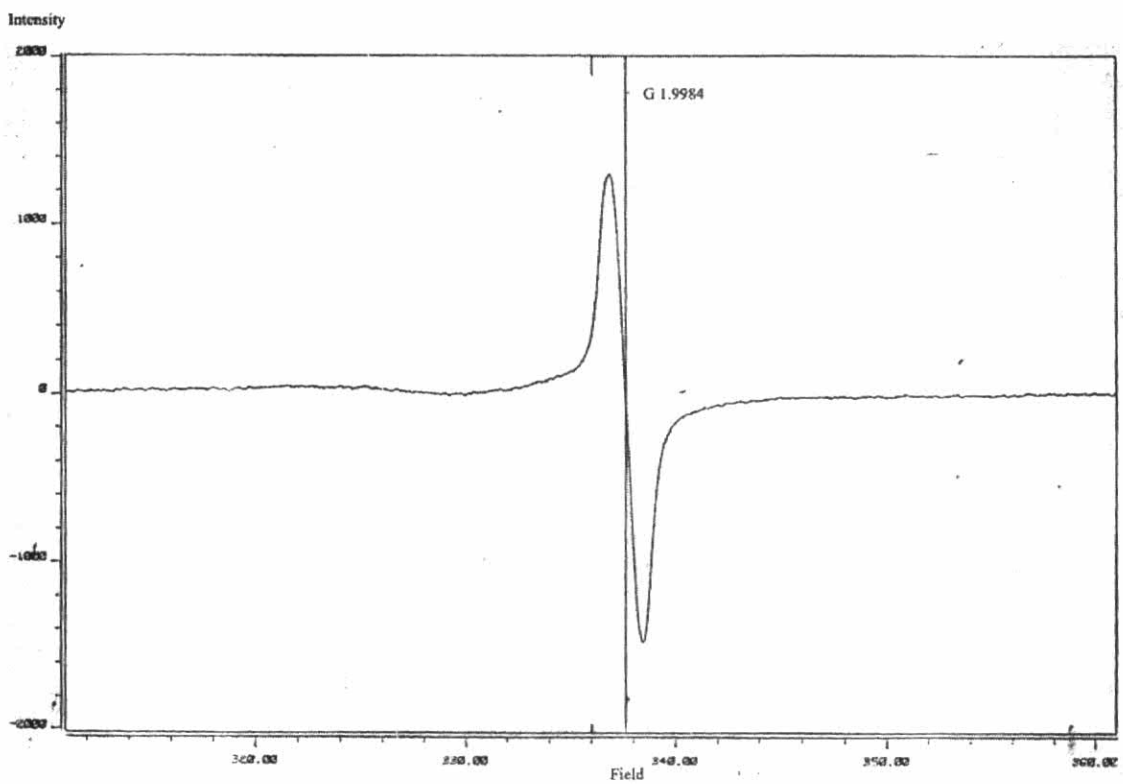

(e)

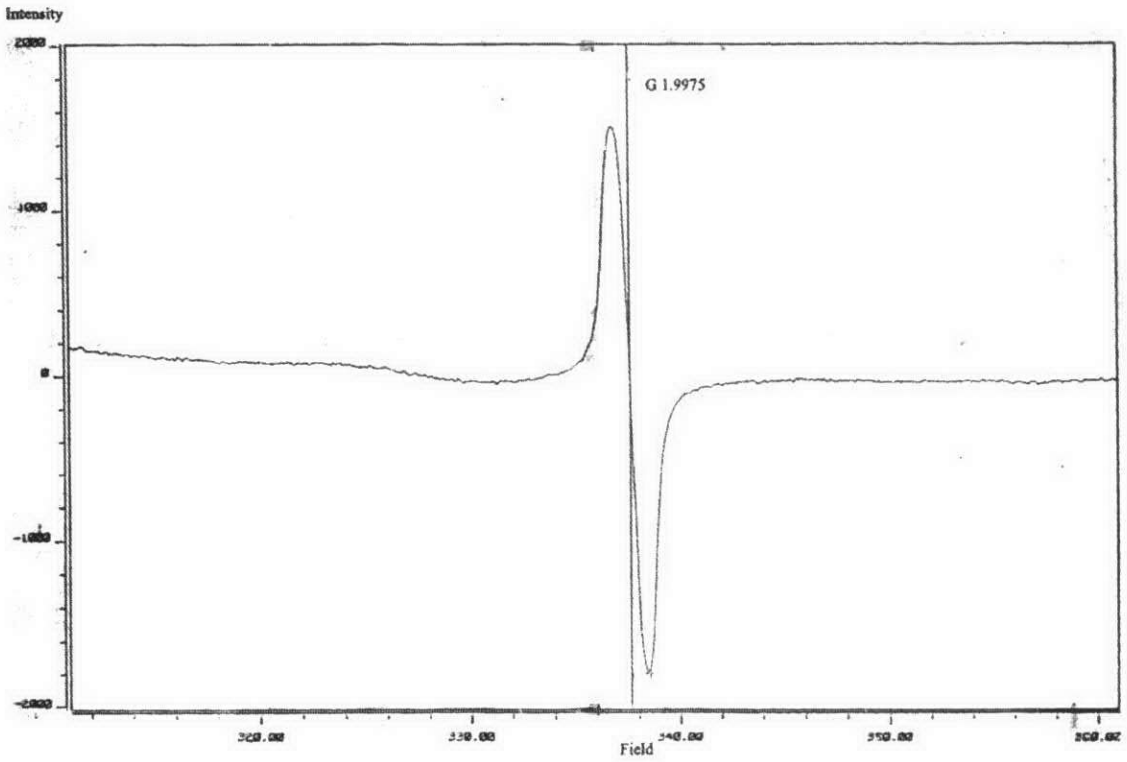

Figure 5.5 ESR spectra for various TiO_2-(a) 9 nm (b) 11 nm samples (c) 12.5 nm (d) 14.5 nm and (e) 15 nm samples.

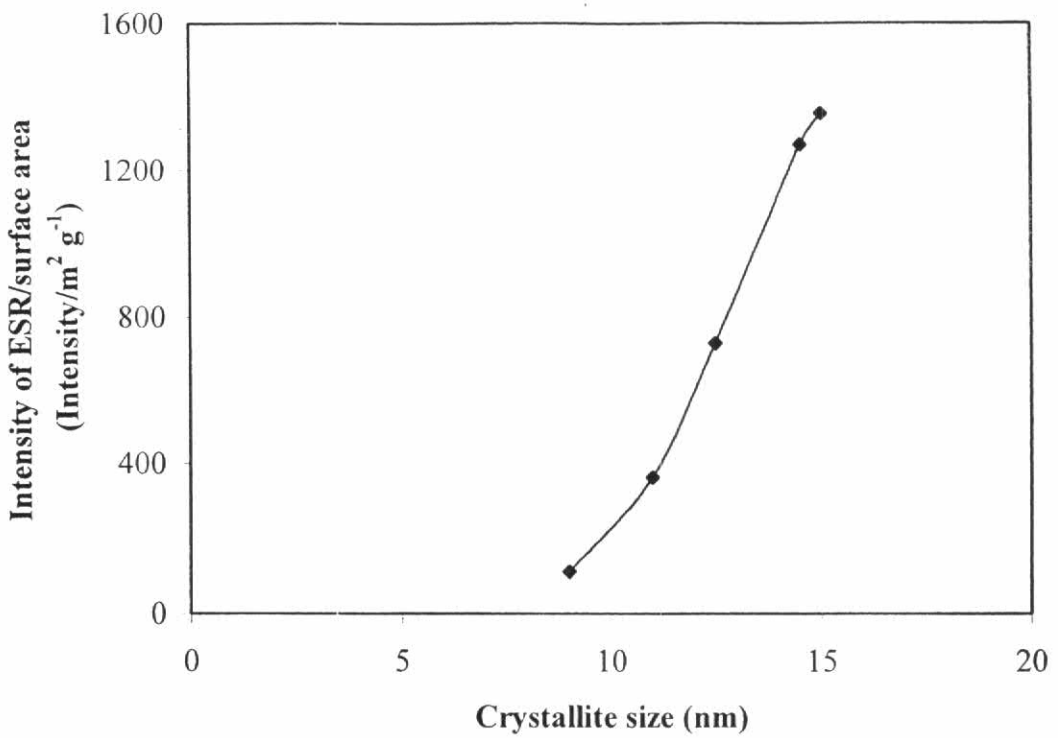

Figure 5.6 The intensity of ESR spectra/surface area as a function of TiO_2 crystallite size.

5.1.6 Photocatalysis reaction

Photocatalytic decomposition of ethylene by using different crystallite size catalysts during photocatalytic decomposition of 1000 ppm ethylene. The flow rate of air was set at 10 ml/min. The photocatalytic reaction operated at room temperature. After switching on the UV lamp of the reactor, photocatalytic reaction started.

Photocatalytic decomposition of ethylene was conducted to assess the photocatalytic activity of the TiO_2 samples with various crystallite sizes. The first 60 minutes of running is the waiting time for system to prepare surface catalyst by feeding of air and irradiation were conducted. After the feeding of ethylene, the conversion of ethylene increases up to the highest conversion and decreases to the conversion at the steady state for 300 minutes operation time. The increase of conversion to the highest value in the initial period operation time due to the amount of species adsorbed on catalyst surface was at the saturated value. After that, a decrease conversion is observed due to the amount of species adsorbed on catalyst surface was decreased. Then, the conversion at the final time of operation was nearly constant due to the equilibrium between the adsorption of gaseous on the catalyst surface and the consumption of surface species.

The conversion of ethylene as a function of time-on-stream for all the samples is shown in **Figure 5.7**. In this study, 'time-on-stream' is defined as the time that surface of the catalyst was illuminated by UV light using 500 W mercury lamps. Photocatalytic activities of the various TiO_2 crystallite sizes are evidently different; ethylene conversions increased with increasing TiO_2 crystallite sizes. It can be correlated to the different amount of Ti^{3+} defects on the TiO_2 samples, in which the higher amount of Ti^{3+} present in TiO_2, the higher photocatalytic activity was obtained. In photocatalysis, light irradiation of TiO_2 powder with photon energy larger than the band-gap energy produces electrons (e^-) and holes (h^+) in the conduction band and the valence band, respectively. These electrons and holes are thought to have the respective abilities to reduce and oxidize chemical species adsorbed on the surface of TiO_2 particles. For a photocatalyst to be most efficient, different interfacial electron processes involving e^- and h^+ must compete effectively with the major deactivation processes involving e^-–h^+ recombination. In general, TiO_2 with higher crystallinity

and higher specific surface area typically shows higher photocatalytic activity since the defect of crystal can be the recombination center of electron-hole pair; hence the photocatalytic activity decreases [Ohtani *et al.* (1998), Jung *et al.* (1999), Litter *et al.* (1999)]. However, the role of Ti^{3+} surface defects on photocatalytic activity of TiO_2 is different from that of crystal (bulk) defect. The Ti^{3+} surface defects serve as traps for photogenerated-electron and consequently prolong lifetime of holes resulting in higher photocatalytic activity [Linsebigler *et al.* (1995), Schwitzgebel *et al.* (1995), Brinkley *et al.* (1998)].

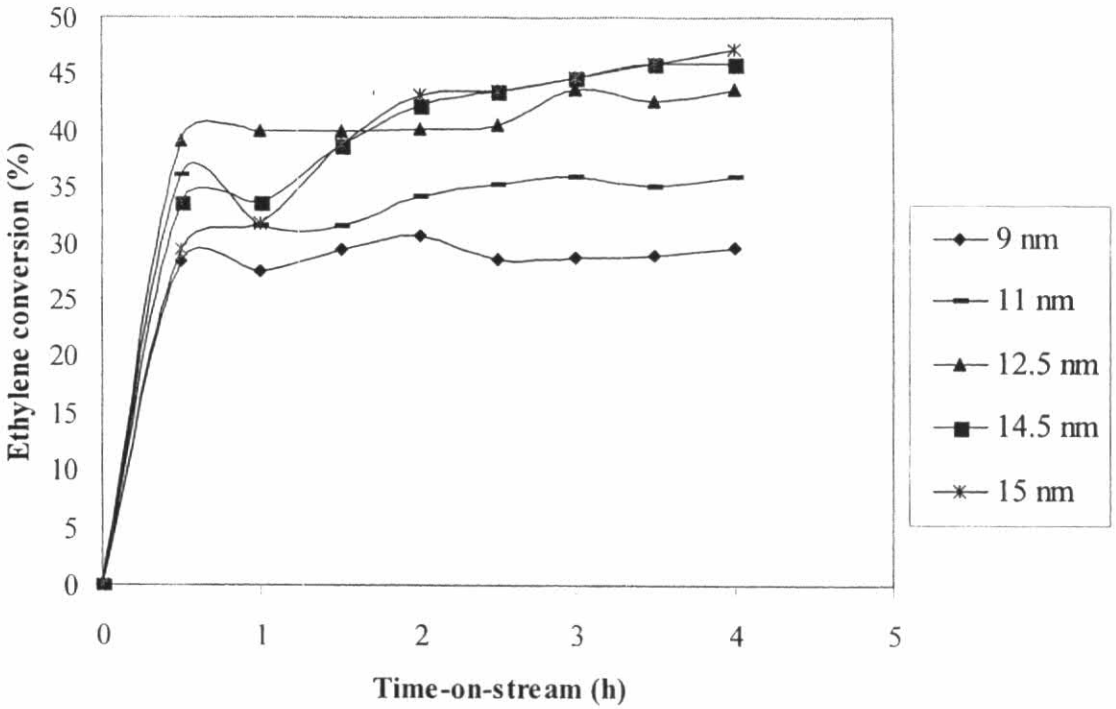

Figure 5.7 Photocatalytic activity of the various TiO_2.

5.2 Formation of 20 wt% of Co/TiO_2

5.2.1 Catalyst Characterization

5.2.1.1 Specific Surface Area

BET surface areas of crystallite sizes of titania unsupported and supported Co catalysts are also shown in Table 5.3. BET surface areas of titania decreased from 126 m^2/g for 9 nm sample to 51 m^2/g for 15 nm sample. After loading 20 %wt Co, the BET surface areas of cobalt supported on titania were lower than the BET surface area of the unsupported titania. BET surface areas of titania-supported Co catalysts were found in the range of 20-42 m^2/g. The significant decrease in surface area of the original support material suggests that cobalt was deposited significantly in the pores of TiO_2.

Table 5.3 BET surface area measurement of titania unsupported and supported Co catalysts.

Sample	Preparation conditions			Average crystallite size	Specific surface area before cobalt loading	Specific surface area after cobalt loading
	TNB amount (g)	Temp. (°C)	Holding time (h)	(m^2/g)	(m^2/g)	(m^2/g)
1	15	300	0.5	9.0	126	41.7
2	25	300	2	11.0	92	34.0
3	25	320	6	12.5	78	30.0
4	25	350	6	14.5	53	21.2
5	25	350	8	15.0	51	20.9

5.2.1.2 Temperature programmed reduction (TPR)

TPR was performed in order to identify the reduction behaviors and reducibility of catalysts. TPR profiles for all samples are shown in Figure 5.8. TPR of the titania support samples used was also conducted at the same TPR conditions used for the catalyst samples and no hydrogen consumption was detected. This indicated that the titania supports used themselves were not reducible at these TPR conditions. Apparently, TPR profiles of all calcined samples were similar exhibiting only one strong reduction peak as shown in Figure 5.8. This peak can be assigned to the overlap of two-step reduction of Co_3O_4 to CoO and then to Co^0 (Kraum and Baern, 1999; Jongsomjit *et al.*, 2001). Upon the TPR conditions, the two reduction peaks based on the two-step reduction may or may not be observed. The only one reduction peak during TPR for all catalyst samples indicated that no residual cobalt nitrates precursor remains on the samples upon the crystallite sizes used in this study.

It was found that the TPR peak around located at ca. 873 K was observed for every samples. However, this reduction peak was dramatically shifted about 25-50 K lower when increased crystallite size. Besides reduction behaviors obtained from TPR results, reducibilities of samples can be measured based on the peak areas below TPR curve (calibrated using Ag_2O), which are related to the amounts of hydrogen consumed during TPR (Kogelbaue *et al.*, 1995; Zhang *et al.*, 1999). The reducibilities during TPR at temperature 35-800°C of titania-supported Co catalysts are shown in Table 5.4. The reducibilities were ranged between 34 to 54% which decreased when the crystallite size of titania increased. The reducibilities decreased when the calcined samples were reduced and performed TPR indicating a loss in reducibility of cobalt oxide species after reduction (Jongsomjit *et al.*, 2004).

From results, this suggested that the presence of bigger titania can facilitate the reduction process of cobalt oxide species on the titania support leading to reduction at a lower temperature. Since TPR is more of a bulk technique, it should be noted that the number of reduced Co metal obtained from the TPR measurement might not be well representative of the number of reduced Co metal surface atoms available for catalyzing CO hydrogenation. The results were consistent with Jongsomjit *et al.* (Jongsomjit *et al.*, 2005). They studied the dependence of crystalline

phases in titania on catalytic properties during CO hydrogenation of Co/TiO_2 catalysts. They reported that pure anatase phase in titania-supported Co catalyst has a stronger interaction between cobalt and titania support due to the shift of a reduction peak to a higher temperature. For the mix phase in titania-supported Co catalyst, they found that there was no significant shift of the reduction temperature upon the hydrothermal treatment during reduction indicating a lesser degree of cobalt-support interaction compared to another one. They suggested that the presence of rutile phase in titania support result in an increase in stability of the titania support. An increase in stability could be the cause for a difficulty of cabalt to interact with it. Moreover, they indicated that the loss in reducibilities can be probably attributed to a nonreducible (at temperatures < 800°C) "Co-titanate" species formed during standard reduction.

Table 5.4 TPR and H_2 chemisorption results for crystallite sizes of titania-supported Co catalysts.

Catalyst samples (nm)	Reducibility (%) during TPR at 35-800°C[a]	Total H_2 chemisorption (μmol H_2/g_{cat})	Overall Co metal dispersion (%)
9	54.3	0.27	1.5
11	53.4	0.78	4.3
12.5	53.1	0.44	2.5
14.5	34.7	0.96	8.1
15	34.2	2.42	20.8

[a] The reduced samples were recalcined at the original calcination conditions prior to performing TPR.

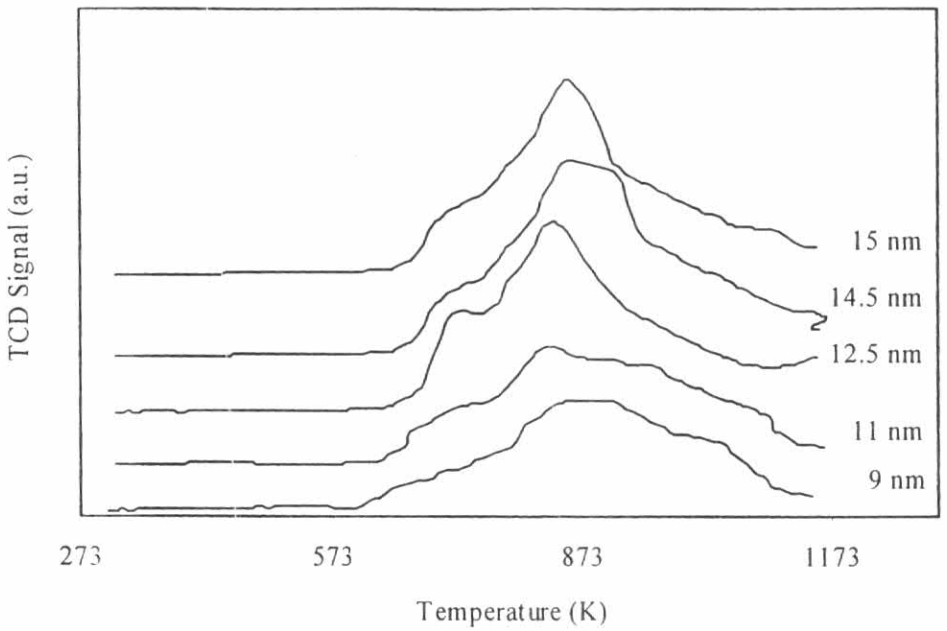

Figure 5.8 TPR profiles of crystallite sizes of titania-supported Co catalysts.

5.2.1.3 H_2 chemisorption

Static H_2 chemisorption on the reduced cobalt catalyst samples was used to determine the number of reduced Co metal surface atoms. This is usually related to the overall activity of the catalyst during CO hydrogenation. H_2 chemisorption was used to determine the number of reduce surface cobalt metal atoms and percentage overall cobalt dispersion. The results of H_2 chemisorption for crystallite sizes of titania-supported Co catalysts are given in Table 5.4. The amounts of H_2 adsorbed increased with the crystallite size in titania increased. Since H_2 chemisorption is a surface technique that the reduced Co metal surface atoms can be measured directly. The amounts of H_2 adsorbed on Co/TiO_2 obtained were lower compared to those for Co/Al_2O_3 and Co/SiO_2 at similar loading (Jongsomjit *et al.*, 2001; Panpranot *et al.*, 2002).

Moreover, the overall Co metal dispersion in the catalyst samples are also shown. The Co metal dispersion of the catalyst samples are given the same result as H_2 chemisorption. However, based on the H_2 chemisorption results, different crystallite size of titania exhibited different amounts of H_2 chemisorbed on the catalyst samples.

5.2.1.4 X-ray diffraction (XRD)

The bulk crystalline phases of samples were determined using XRD. For the pure anatase titania, XRD peaks of the anatase phase of titania at 25◦ (major), 37◦, 48◦, 55◦, 56◦, 62◦, 71◦, and 75◦ were evident.

A 20 wt% of cobalt supported on titania was prepared by the conventional incipient wetness impregnation method and calcination at temperature ca. 773 K for 4 h. The XRD patterns for all samples (Co/TiO_2) are shown in Figure 5.9.

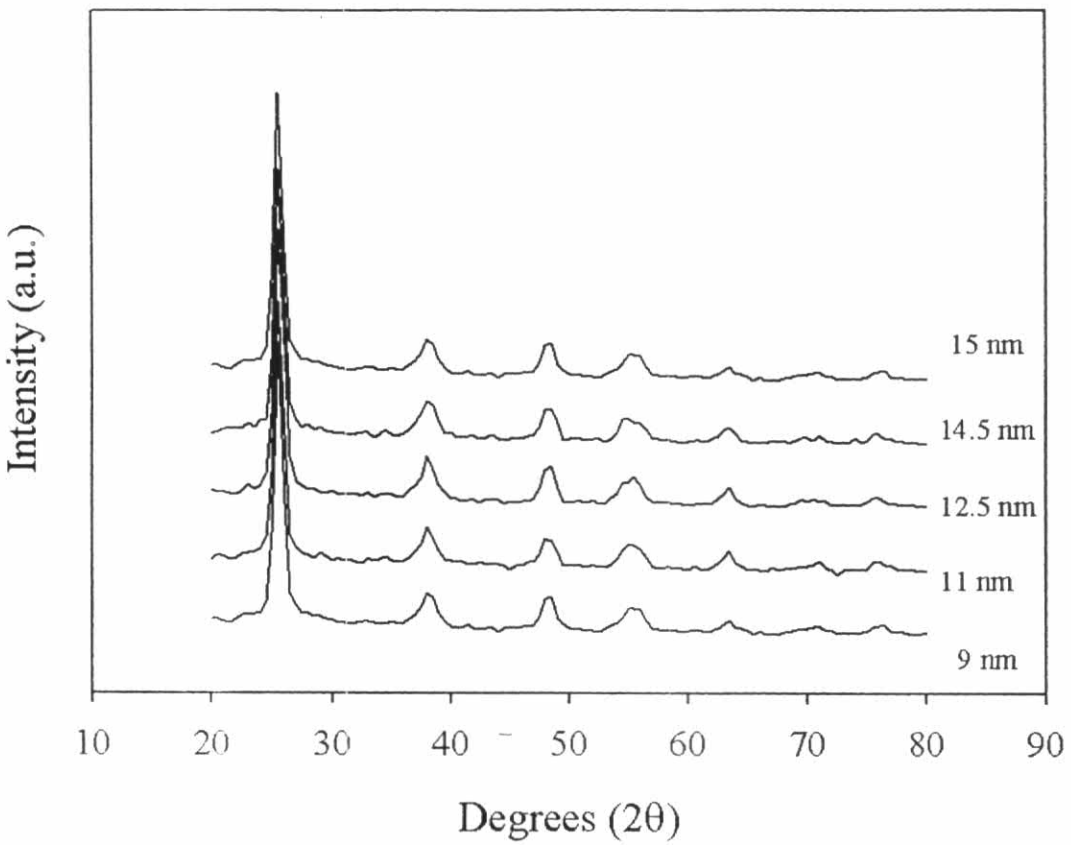

Figure 5.9 XRD patterns of nanocrystalline TiO_2 synthesized by solvothermal method

5.2.1.5 Reaction study in CO hydrogenation

Cobalt is in the form of cobalt oxide phase (Co_3O_4 or Co_2O_3). Cobalt oxide has to be reduced to cobalt metal (Co^0) prior to reaction since cobalt metal is known to be the most active phase for CO hydrogenation, not its oxide. Before reaction, the catalyst was reduced in-situ in H_2 flow 50 cc/min at 350°C for 3 h in order to obtain metallic phase cobalt.

CO hydrogenation was performed in a fixed-bed flow reactor and was carried out at 220°C, 1 atm, and H_2/CO ratio = 10 for all the catalyst samples. A relatively high H_2/CO ratio was used in order to minimize catalyst deactivation due to carbon deposition during reaction. The results are shown in Table 5.5. It indicated that the reaction rate ranged between 6.3 and 8.7 $gCH_2/g_{cat}h^{-1}$. The CO conversion ranged between 2.4 to 3.0 %. This also showed that activities of the samples increased with crystallite size of titania increased.

Table 5.5 Reaction rate for CO hydrogenation on the crystallite size of titania-supported Co catalysts.

Samples (nm)	CO conversion (%)	Rate($\times 10^2 gCH_2/g_{cat}h^{-1}$)
	SS	SS
9	3.0	8.1
11	3.0	8.7
12.5	2.4	6.3
14.5	3.1	8.0
15	3.1	8.3

5.2.1.6 Electron microscopy

SEM were also conducted in order to study the morphologies of the catalyst samples, respectively. The typical SEM micrographs are illustrated in Figure 5.10 for the all of titania-supported Co catalysts samples. The external surface of catalyst granule is shown in all figures and the light or white patches (the term "patches" is used to refer the entities rich in cobalt supported on the catalyst granules) on the catalyst granule surface represent high concentration of cobalt oxides species on the surface. It can be seen that the cobalt oxide species were well dispersed on increased crystallite size of titania.

(a)

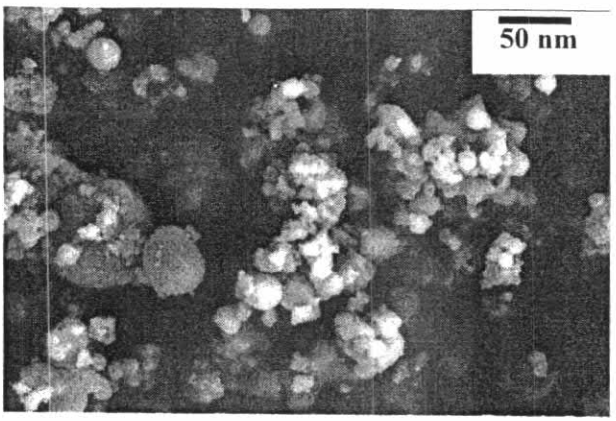

(b)

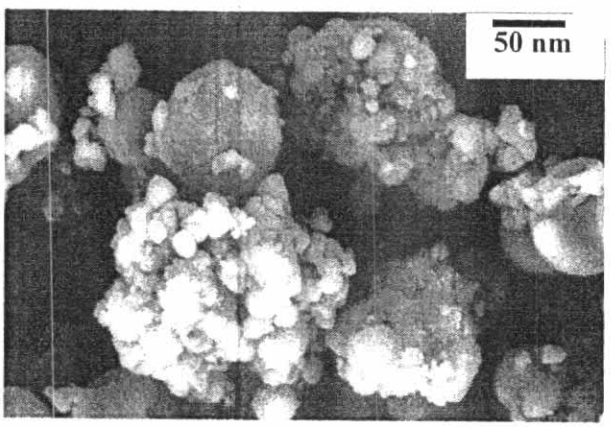

(c)

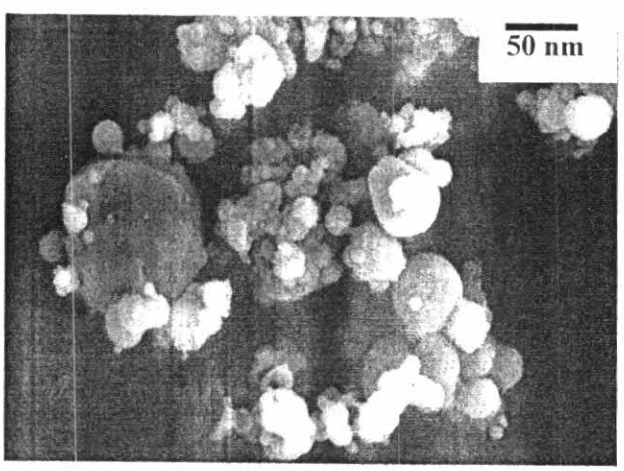

(d)

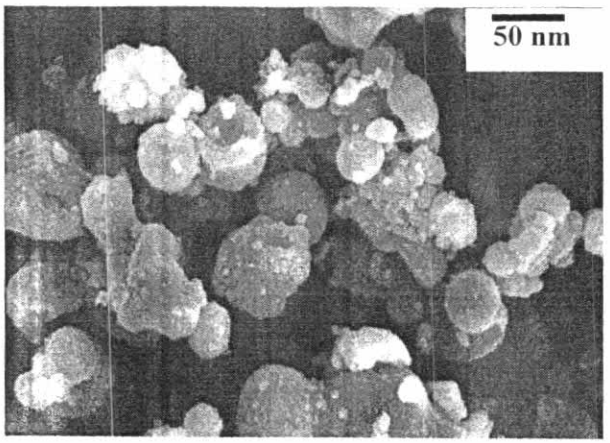

(e)

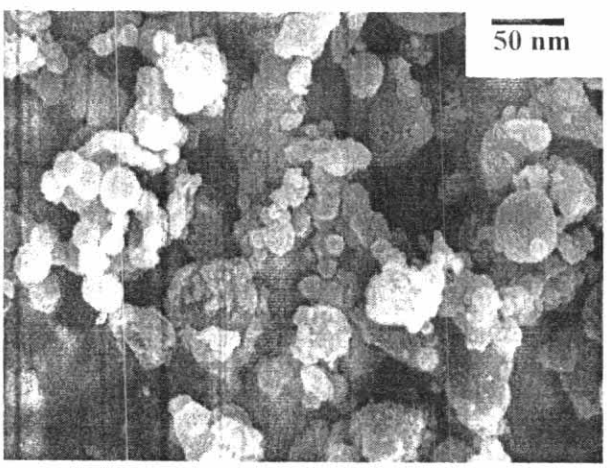

Figure 5.10 SEM micrographs of 20 wt% Co supported on TiO_2-(a) 9 nm (b) 11 nm (c) 12.5 nm (d) 14.5 nm and (e) 15 nm.

5.2.1.7 Transmission Electron Microscopy (TEM)

TEM micrographs were taken for all the catalysts in order to physically measure the size of cobalt oxide particles and/or cobalt clusters. The TEM micrographs for all samples are shown in Figure 5.11. The dark spots represented cobalt oxide species dispersing on titania. It can be observed that cobalt oxide species were highly dispersed on the titania supports for 9, 11, 12.5, 14.5, and 15 nm samples resulting in an appearance of smaller cobalt oxide patches present. However, the degree of dispersion for cobalt oxide species essentially increased with increasing of crystallite size of titania samples resulting in the observation of larger cobalt oxide patches.

(a)

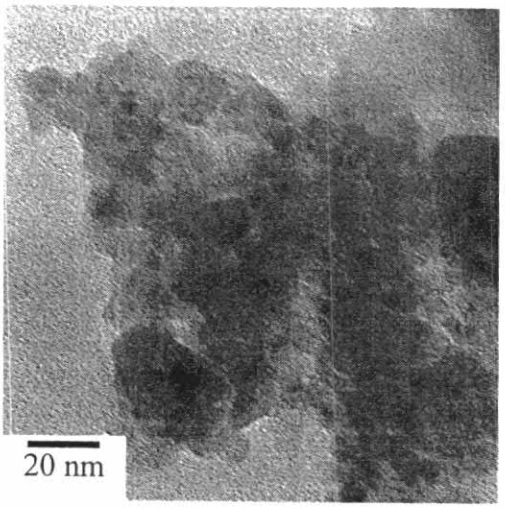

(b)

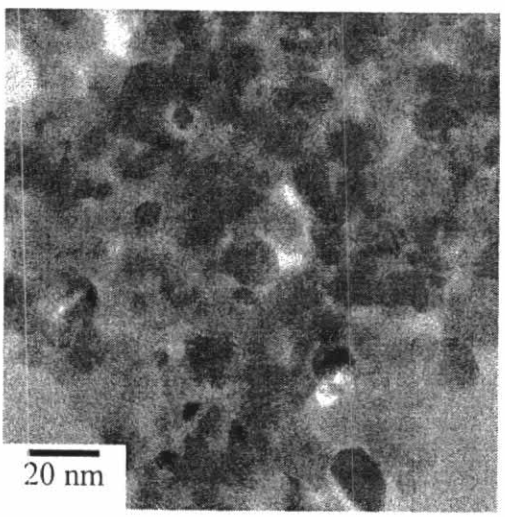

(c)

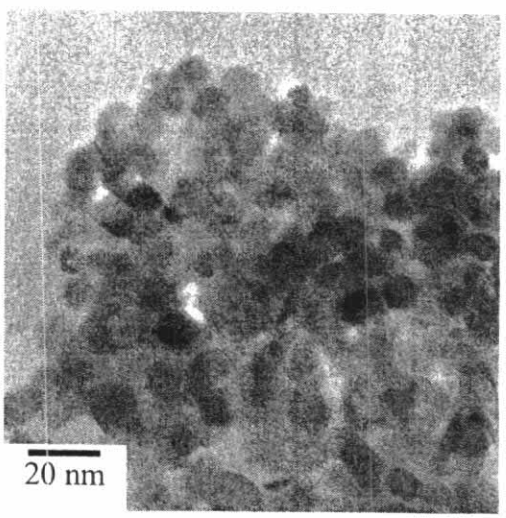

(d)

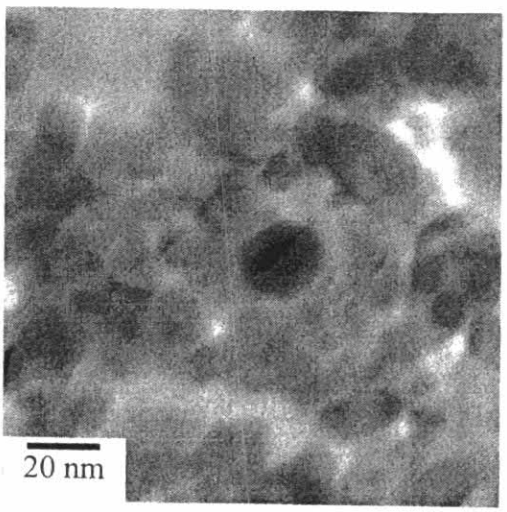

(e)

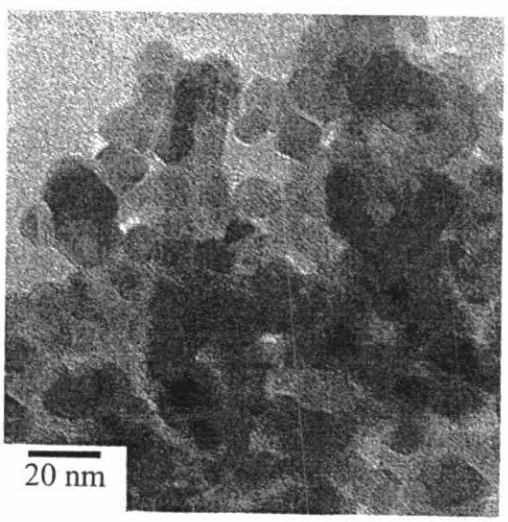

Figure 5.11 TEM micrographs of 20 wt% Co supported on TiO_2-(a) 9 nm (b) 11 nm (c) 12.5 nm (d) 14.5 nm and (e) 15 nm.

5.3 Formation of various cobalt dispersion onTiO_2

5.3.1 Catalyst Characterization

5.3.1.1 Specific Surface Area

The results of BET surface area of various cobalt dispersion on titania catalysts analyzed be N_2 adsorption are summarized in **Table 5.6**.

The data in Table 5.6 indicated that impregnation of cobalt onto the titania supports decreased the surface area of titania support. Moreover, when various cobalt loading on titania, the surface area was further decreased, percentage of cobalt loading increased, suggesting that some of the pores of titania support were blocked by the metal. The specific surface areas decreased when % Co loading increased from 5 to 20 wt. % suggesting that cobalt was deposited in the pores of the TiO_2 supports. It should be noticed, that the reduction of the specific surface area of Co catalysts on TiO_2 - 9 nm was not as much as that observed for the TiO_2 - 15 nm.

Table 5.6

The characteristics of the supports and catalyst samples.

Supports	**BET surface area ($m^2 g^{-1}$)**	**Catalyst Samples**	**BET surface area ($m^2 g^{-1}$)**
Ti9	126.4	5 wt.% Co/Ti9	55.6
		10 wt.% Co/Ti9	50.5
		15 wt.% Co/Ti9	47.4
		20 wt.% Co/Ti9	41.7
Ti15	51.1	5 wt.% Co/Ti15	40.1
		10 wt.% Co/Ti15	35.2
		15 wt.% Co/Ti15	27.3
		20 wt.% Co/Ti15	20.9

5.3.1.2 Catalyst Structure and Particle Size Distribution

X-ray diffraction analysis was used to determine the bulk crystallite phase in the catalysts. The XRD patterns of 5, 10, 15, and 20 wt% Co/TiO_2 catalysts are depicted in Figure 5.12.

XRD patterns obtained for the various cobalt dispersion on Co/TiO_2 - 9 nm and Co/TiO_2 - 15 nm samples are displayed in Fig. 1, the peaks of titania for all the samples at 25, 38, 48, 55, 56, 62, 69, 71 and 79° 2θ [Suriye et al., 2005; Kim, 2005], the diffraction peaks of Co_3O_4 at 36°, 46°, and 65° can be observed. Jongsomjit et al. [Jongsomjit et al., 2004; Kraum et al., 1999] reported XRD peaks of $CoTiO_3$ at 23°, 32°, 35°, 49°, 52°, 62°, and 64°. In the X-ray diffraction patterns of Co/TiO_2 catalysts, only pure anatase phase TiO_2 was observed and the XRD diffraction peaks for cobalt oxide (Co_3O_4) were not clearly seen for all the catalyst samples.

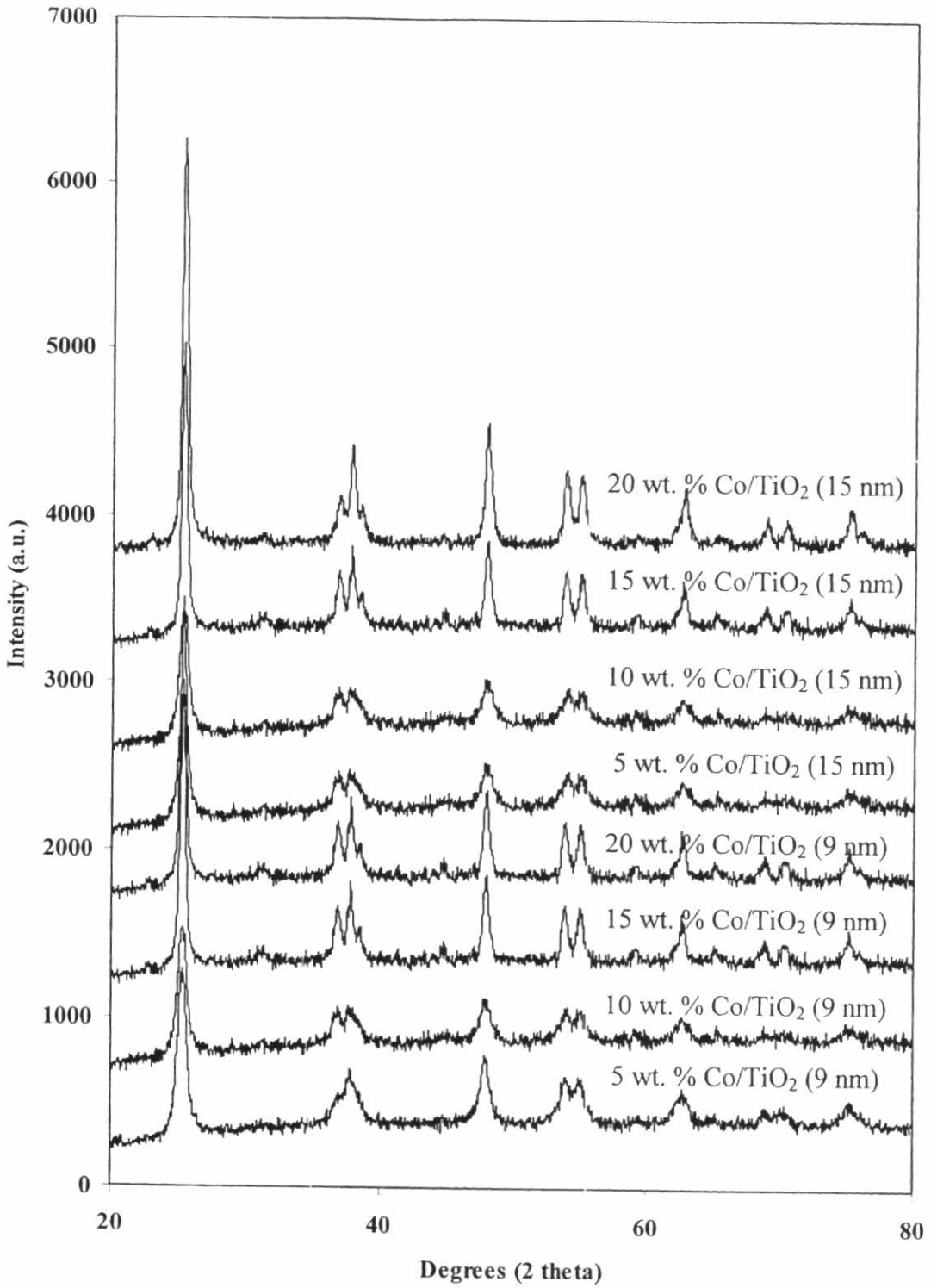

Figure 5.12 XRD patterns of the Co/TiO_2 samples (9 and 15 nm) with various cobalt loading.

5.3.1.3 Metal Active Sites

H_2 chemisorption technique provides the information on the number of cobalt active sites and percentages of metal dispersion. The total H_2 uptakes and the percentages of cobalt metal dispersion are reported in Table 5.7

High degree of reduction and high cobalt metal dispersion are considered to be two of the most important factors for designing CO hydrogenation catalysts. The %Co dispersion, H_2 chemisorption results, and CO hydrogenation rates are given in **Table 5.7** and **Table 5.8**. The H_2 chemisorption results revealed that increasing cobalt loading (from 5 to 20 wt. %) yielded lower cobalt dispersion for both TiO_2 – 9 nm and TiO_2 – 15 nm supports. However, for the similar percent Co loading, the larger titania size gave higher % Co dispersion. In order to distinguish the effect of crystallite size of TiO_2 and the effect of surface area, we also report the H_2 chemisorption results in terms of the amount of H_2 adsorbed per total surface area of the catalyst (see **Figure 5.13**). For the 9 and 15 nm size titania support catalysts, the number of active surface cobalt metal atoms per unit surface area increased with increasing Co loading up to 10 wt. %. Further increase of the amount of Co loading to 20 wt. % resulted in both a lower cobalt dispersion and fewer exposed surface cobalt metal atoms. This is typical for supported Co Fischer-Tropsch catalysts. Dispersion usually decreases with increasing Co loading beyond a certain point [Wei-xing et al., 1995]. To study the effect of crystallite size on active sites of Co catalyst, TiO_2 - 15 nm support was characterized to compare with TiO_2 - 9 nm support, that the amounts of H_2 adsorbed increased from 1.5 to 5.4 $\times$ 10^{18} molecules/g catalyst. While the amounts of H_2 adsorbed of 9 nm size titania catalyst ranged around 0.16 to 1.19 $\times$ 10^{18} mol/g catalyst. Therefore, it can be concluded that for any Co loading, Co dispersion was higher when larger crystallite size of TiO_2 was used as support for Co/TiO_2 catalyst. The catalyst activities and selectivities in CO hydrogenation are also given in **Table 5.8.** Considering selectivity to methane, it was found that the presence of %Co loading and crystallite size in titania resulted in an increased selectivity to methane. A similar trend of the results of H_2 chemisorption was observed for the catalyst activities that the catalysts activities increased with increasing Co loading from 5 wt. % to 10 wt. % and then started to decrease when further increase Co loading to 15 and 20 wt.

%. The CO hydrogenation rates showed maximum values at 10 wt% Co loading with the lowest values for the 20 wt. % Co loading. Since only Co metal has significant activity for CO hydrogenation, these results are consistent with both the reducibility and H_2 chemisorption results. The corresponding trend of the CO hydrogenation rates and the H_2 chemisorption results was seen for both sizes of the titania supports.

Table 5.7

TPR and H_2 chemisorption results for various of Co loading of titania-supported Co catalysts.

Catalyst	H_2 chemisorption ($\times 10^{18}$ mol g cat^{-1})	Reducibility (%) TPR at 308-1073 K	Overall Co metal dispersion[a] (%)	d_p Co^0 (nm) = (94/%D)
5 wt.% Co/Ti9	0.2	32.3	1.94	48.4
10 wt.% Co/Ti9	1.2	35.6	0.87	108.3
15 wt.% Co/Ti9	0.5	62.6	0.58	162.5
20 wt.% Co/Ti9	0.2	61.8	0.43	216.7
5 wt.% Co/Ti15	5.0	57.6	2.58	36.5
10 wt.% Co/Ti15	5.4	66.8	1.47	64.0
15 wt.% Co/Ti15	2.9	75.1	0.98	95.9
20 wt.% Co/Ti15	1.5	78.1	0.73	127.9

[a] % Co dispersion = [2 × (total H_2 chemisorption/g cat.) / (no. of μmol of Co total/g cat.)] × 100 %.

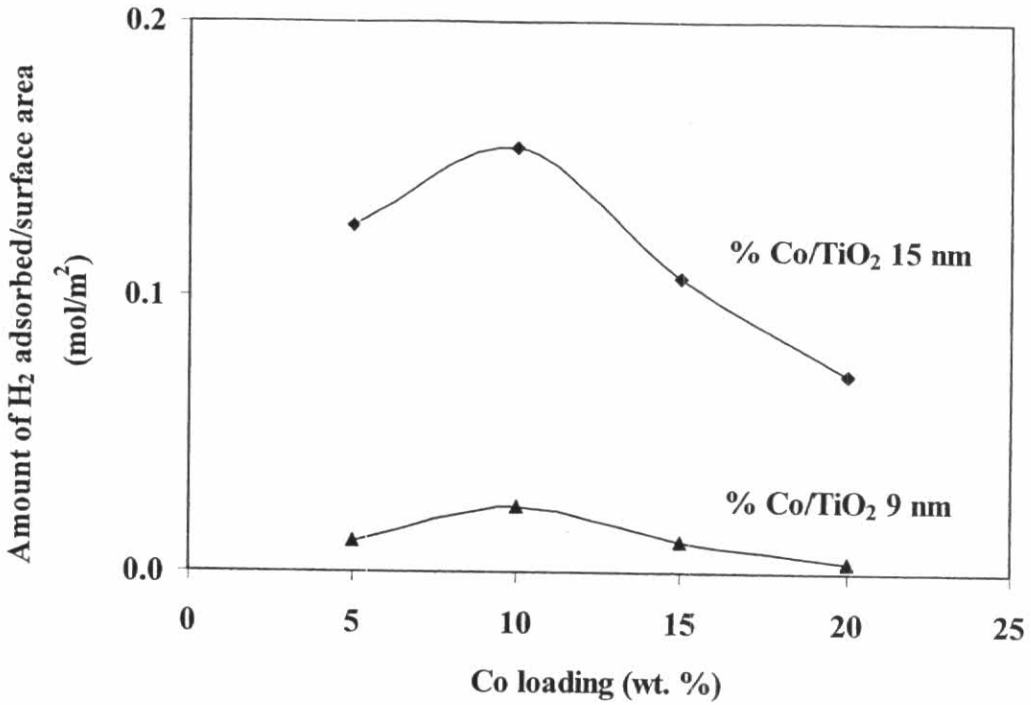

Figure 5.13 The amount of H_2 chemisorption/specific surface area of the Co/TiO_2 catalysts as a function of cobalt loading.

5.3.1.4 Transmission Electron Microscopy (TEM)

The study of morphology of the Co/TiO_2 catalysts was also carried out using Transmission Electron Microscope (TEM). Figure 5.14 and 5.15 depict TEM micrographs of Co catalysts supported on titnia synthesized in toluene. The average crystallite size of titania for cobalt support observed from TEM were found to be increased particle, cobalt dispersion was better. For the same size of support, when percentage of cobalt up, the dispersion decreased, the cobalt precipitate increased.

(5 wt. %)

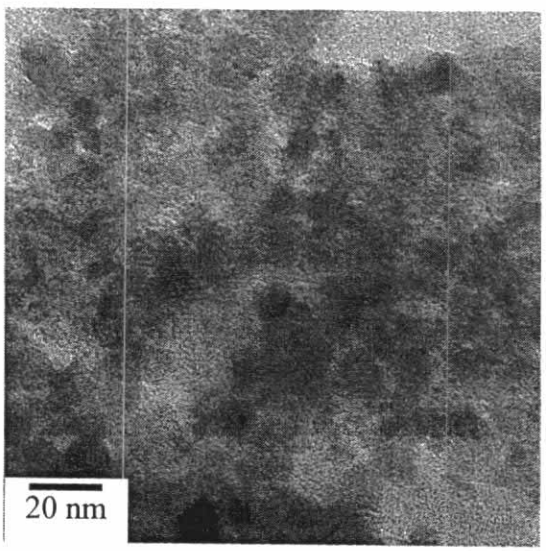

(10 and 15 wt. %)

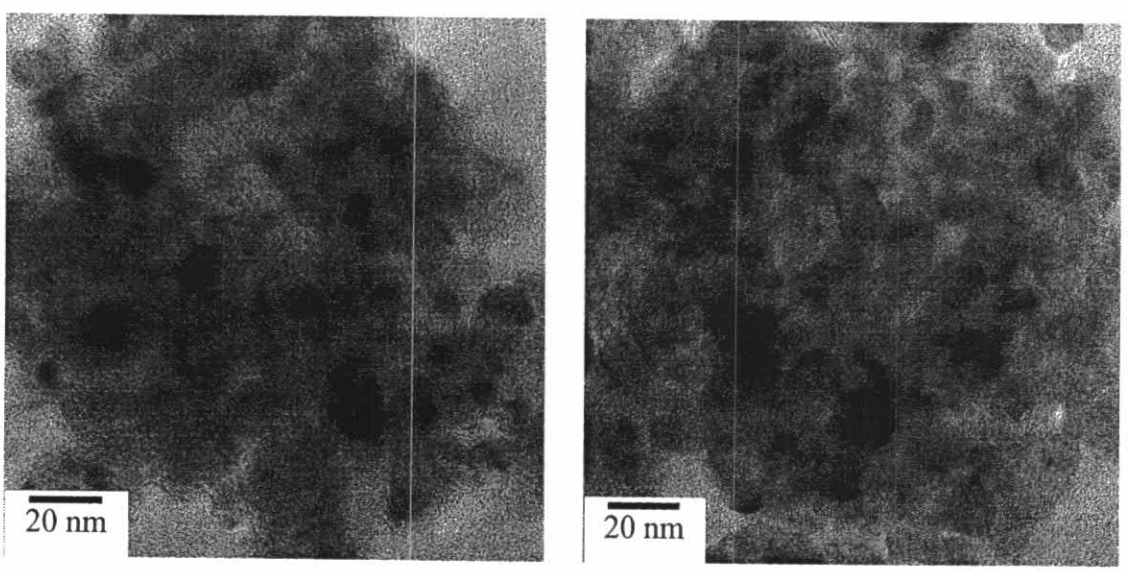

Figure 5.14 TEM micrographs of 5, 10, and 15 wt. % Co supported on TiO_2 - 9 nm

(5 wt. %)

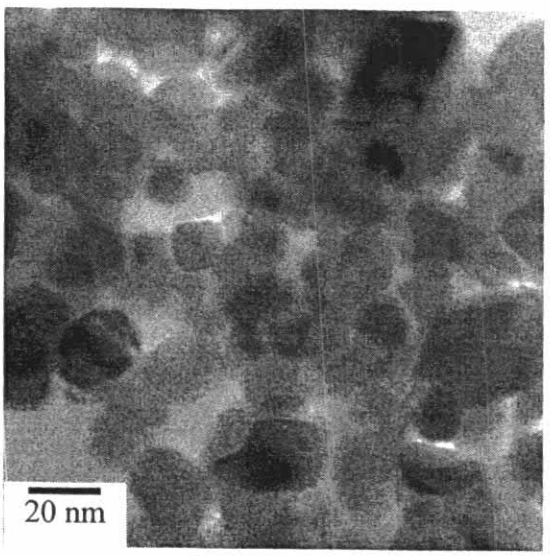

(10 and 15 wt. %)

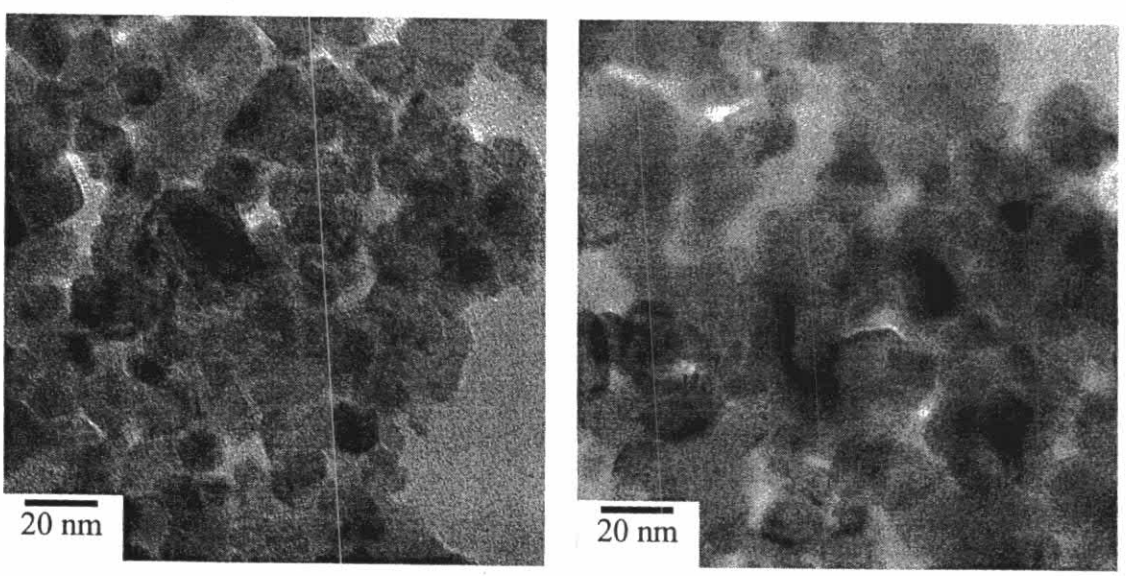

Figure 5.15 TEM micrographs of 5, 10, and 15 wt% Co supported on TiO_2 - 15 nm

5.3.1.5 Electron microscopy

SEM were also conducted in order to study the morphologies of the catalyst samples, respectively. The typical SEM micrographs are illustrated in Figure 5.16 and 5.17 for the all of titania-supported Co catalysts samples.

SEM were performed to study the morphologies of the catalyst samples. SEM micrographs of Co/TiO_2 are shown in Figure 3. In all the SEM figures, the white or light spots on the catalyst granules represent high concentrations of cobalt and its compounds, where the darker areas of the granules indicate the support with no cobalt present. The typical overall shapes of the granules of the catalysts were sphere. There was no significant change in morphologies of the TiO_2 supports upon the presence of cobalt. It can be seen in figure 3 that Co on the 20 wt. % Co/TiO_2 catalyst was most cumulative on the titania support more than the other wt. % Co/TiO_2 catalysts suggesting the lowest Co dispersion. **Table 5.8** shows related of dispersion and crystallite diameter (in nm) that the dispersion exposed increases with decreasing the diameter of cobalt oxide particles. So in Figure 3, we can be seen 20 wt. % Co/TiO_2 catalyst was biggest than the other wt. % Co/TiO_2 catalysts.

(5 wt. %)

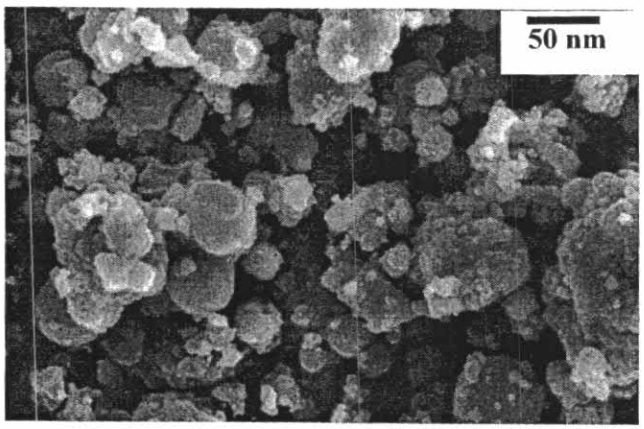

(10 wt. %)

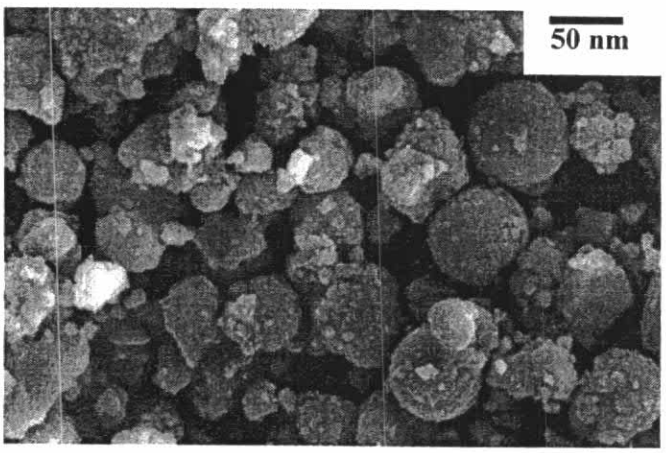

(15 wt. %)

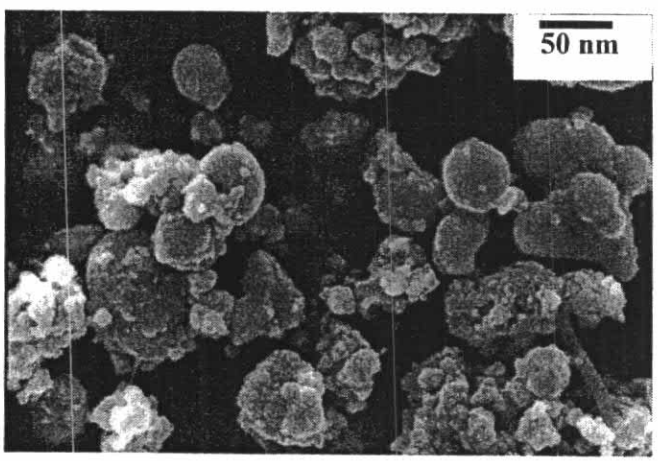

Figure 5.16 SEM micrographs of 5, 10, and 15 wt% Co supported on TiO_2-9 nm

(5 wt. %)

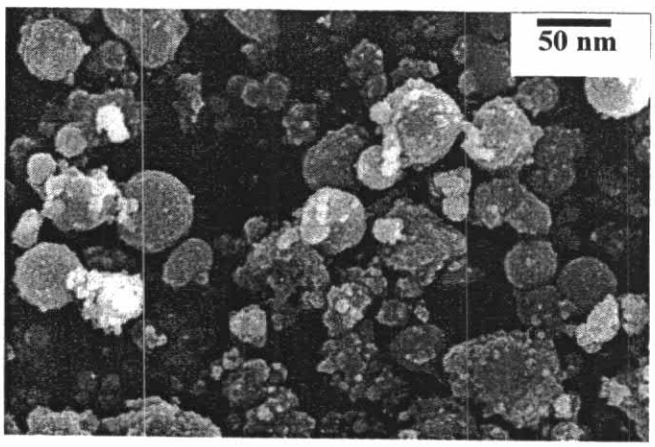

(10 wt. %)

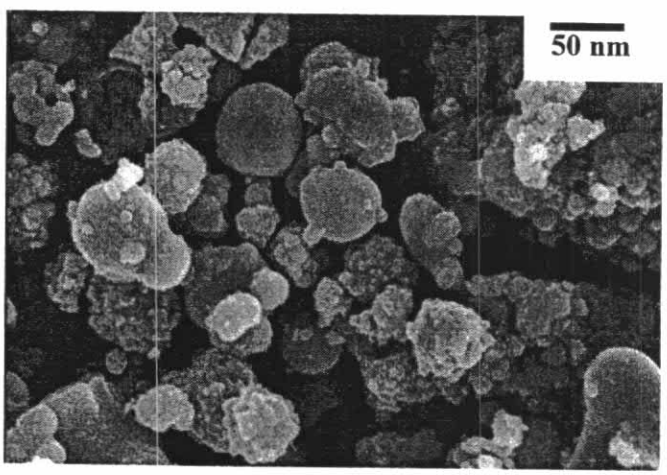

(15 wt. %)

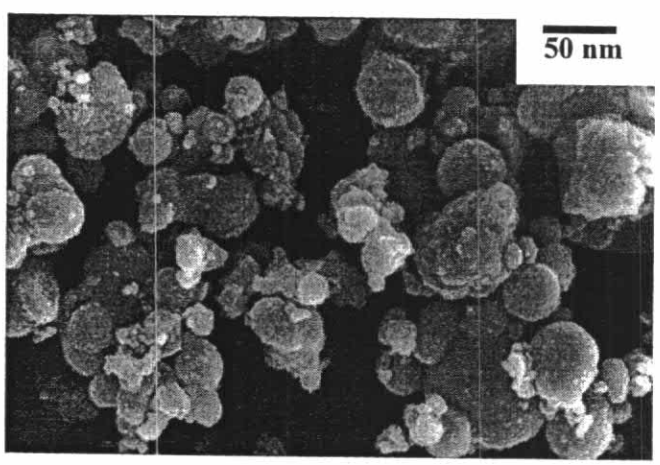

Figure 5.17 SEM micrographs of 5, 10, and 15 wt. % Co supported on TiO_2-15 nm

5.3.1.6 Temperature programmed reduction (TPR)

Since the active phase of cobalt for CO hydrogenation is Co^0 metal not its oxide or carbide, high reducibility of the catalyst is required in order to obtain the catalyst has high activity. The reduction behaviors of the various Co/TiO_2 were investigated by means of temperature-programmed reduction (TPR). Figure 5.18 shows the TPR profiles of all the samples. The reduction zone started at about 573 K and ended at around 1000 K. The first observable reduction peak at 573-693 K could be attributed to the reduction of trivalent Co to divalent Co as shown in Eq. (1), assuming pure Co_3O_4 initially existed. The stronger signal at 693-900 K could be traced back to the reduction of CoO to metallic Co, as Eq. (2). The reduction of Co_3O_4 particles to metallic cobalt (Co^0) through the CoO step has been suggested by many authors [Kraum et al., 1999; Zhang et al., 1999; Schanke et al., 1995; Jongsomjit et al., 2001]

$$Co_3O_4 + H_2 \longrightarrow 3CoO + H_2O \quad (1)$$

$$CoO + H_2 \longrightarrow Co + H_2O \quad (2)$$

For a similar Co loading, it was found that, the reduction temperatures of the Co catalysis supported on TiO_2 - 9 nm were slightly shifted to lower temperature when compared to those of Co/TiO_2 - 15 nm. The higher temperature reduction peak indicated that cobalt on the TiO_2 – 15 nm could interact stronger with the support. In other words, the reduction to metallic cobalt was easier in the case of TiO_2 - 9 nm.

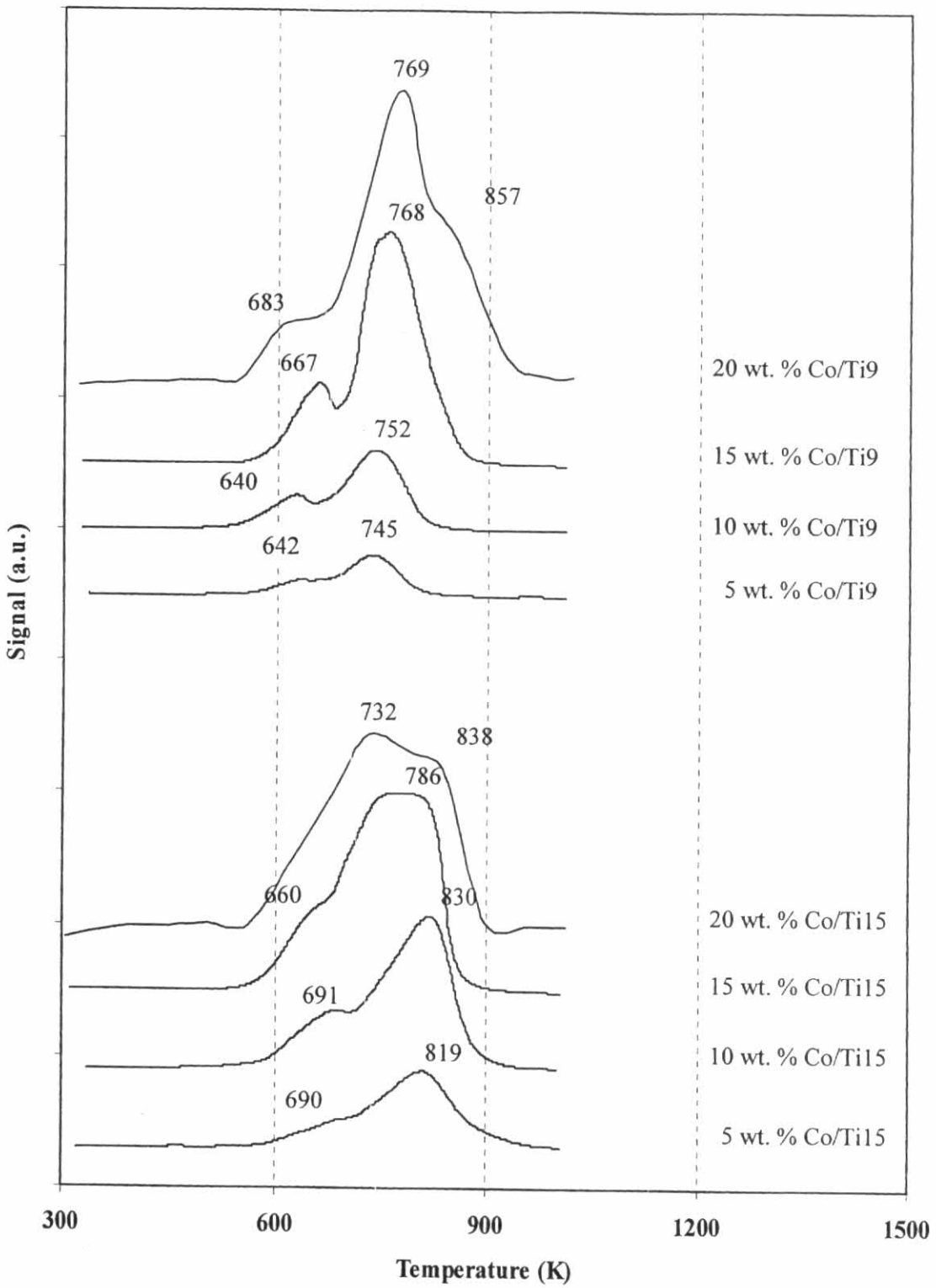

Figure 5.18 TPR profiles of crystallite sizes of titania-supported Co catalysts.

5.3.1.7 Reaction study in CO hydrogenation

CO hydrogenation is a mean to convert synthesis gas obtained from natural gas reforming and coal gasification, into mainly desirable long chain hydrocarbons. The main reactions of CO hydrogenation are [Calvin et al., 2005],

$$CO + [1+(m/2n)]H_2 \longrightarrow (1/n)C_nH_m + H_2O \quad (3)$$

$$CO + 3H_2 \longrightarrow CH_4 + H_2O \quad (4)$$

$$CO + H_2O \longrightarrow CO_2 + H_2 \quad (5)$$

$$2CO \longrightarrow C + CO_2 \quad (6)$$

Eq. 3 is the formation of hydrocarbons of the chain length higher than C1, and Eq. 4 is methanation. The water-gas shift reaction, which is undesirable for natural gas conversion, is shown in Eq. 5. The Boudouard reaction, which results in carbon deposition on the catalyst surface, is shown in Eq. 6. Depending upon the type of catalyst used, promoters, reaction conditions (pressures, temperatures, and H_2/CO ratios), and type of reactors, the distribution of the molecular weight of the hydrocarbon products can be noticeably varied.

The resulted reaction study is also shown in **Table 5.8**. As expected, based on the H_2 chemisorption results, the overall activities for initial dramatically increased up to 10 wt% and decreased to 20 wt% cobalt dispersion on titania supports.

The reducibilities of the catalyst samples can be measured based on the peak area below TPR curve (calibrated using Ag_2O), which are related to the amounts of hydrogen consumed during TPR [Zhang et al., 1999; Kogelbaue et al., 1995]. The reducibilities during TPR at temperature 308-1073 K of the various Co dispersion of titania-supported Co catalysts are shown in **Table 5.7**. For any given size of the TiO_2 support, reducibilities of the catalyst samples increased with increasing of Co loading. Similar behavior was also observed by other authors [Jongsomjit et al., 2002 and 2001; Batista et al., 2006; Feller et al., 1999]. For a similar Co loading, the reducibility of the Co catalysts supported on TiO_2 – 9 nm and TiO_2 – 15 nm were not significantly different ranging from 32.3 – 78.1 % as Co loading increased from 5 to 20 wt. %.

Table 5.8

The catalytic activities of the titania supported Co catalysts for CO hydrogenation reaction

Catalyst	Reaction rate[a] ($g\ CH_2\ g\ cat^{-1}\ h^{-1}$)	Product selectivity (%)	
		CH_4	C_2-C_{4+}
5 wt.% Co/Ti9	0.7	84.5	15.5
10 wt.% Co/Ti9	1.5	98.3	1.7
15 wt.% Co/Ti9	1.3	91.6	8.4
20 wt.% Co/Ti9	1.1	86.8	13.2
5 wt.% Co/Ti15	8.5	88.7	11.3
10 wt.% Co/Ti15	37.1	98.9	1.1
15 wt.% Co/Ti15	1.3	91.0	9.0
20 wt.% Co/Ti15	1.2	92.4	7.6

[a]Reaction condition were 220 °C, 1 atm, and H_2/CO/Ar ratio = 20/2/8 cc/min.